Visual Neuroscience

ARTICLE

Open Access

https://doi.org/10.48130/vns-0026-0035

Visual Neuroscience **2026**, 43: e038

RPE65 deficiency disrupts inner retinal architecture via impaired VGF signaling in LCA

Sifeng Wang[1#], Jianbo Yang[2#], Xiang Hu[2*] and Xiangwen Peng[1*]

[1] *Changsha Hospital for Maternal and Child Health Care Affiliated to Hunan Normal University, Changsha 410001, China*

[2] *College of Life Sciences, Hunan Normal University, Changsha 410081, China*

[#] Authors contributed equally: Sifeng Wang, Jianbo Yang

[*] Correspondence: huxiang@hunnu.edu.cn (Hu X); pxw1237@163.com (Peng X)

Abstract

Mutations in *RPE65* cause Leber congenital amaurosis (LCA), a condition classically characterized by photoreceptor degeneration; however, its inner retinal involvement remains poorly defined. We identified two Chinese siblings with LCA harboring novel compound heterozygous *RPE65* variants (p.Glu399*/p.Pro467Ala) who exhibited night blindness and atypical white dot-like fundus lesions. To investigate the underlying pathogenic mechanisms, we generated an *Rpe65* p.Pro467Ala knock-in mouse model. Homozygous mutants displayed not only degeneration of the photoreceptor's outer segment but also marked disorganization of the ganglion cell layer (GCL) with an irregular nuclear morphology, extending RPE65's pathology beyond the outer retina. Transcriptomic analysis revealed the downregulation of phototransduction genes and *Vgf*, a neurotrophic factor. Immunofluorescence confirmed significantly reduced VGF nerve growth factor inducible (VGF) protein levels, predominantly in the inner nuclear layer (INL), which spatially correlated with GCL abnormalities. Notably, intravitreal administration of the VGF-derived neuroprotective peptide AQEE-30, delivered every 4 d for 30 d, significantly ameliorated the GCL's structural disorganization without rescuing photoreceptor degeneration, indicating layer-specific neuroprotection. These findings demonstrate that RPE65 deficiency disrupts the inner retinal architecture via impaired VGF signaling, revealing a previously underappreciated pathological dimension of RPE65-associated LCA. The selective rescue of GCL pathology by AQEE-30 provides a proof of concept that augmenting VGF-related pathways may offer an adjunctive neuroprotective strategy to preserve inner retinal neurons in RPE65-associated retinopathy.

Keywords: *RPE65*, Leber congenital amaurosis, Ganglion cell layer, VGF, Knock-in mouse model, Retinal degeneration

Citation: Wang S, Yang J, Hu X, Peng X. 2026. *RPE65* deficiency disrupts inner retinal architecture via impaired VGF signaling in LCA. *Visual Neuroscience* 43: e038 https://doi.org/10.48130/vns-0026-0035

Introduction

Leber congenital amaurosis (LCA) is a group of genetic childhood-onset retinal dystrophies (RDs) with an estimated prevalence of 1:50,000 to 1:100,000[1]. It is characterized by severe vision loss, night blindness, and retinal dysfunction, often leading to complete blindness in early childhood[2–5]. Over 10% of LCA cases are caused by mutations in the *RPE65* gene, which encodes a critical enzyme in the retinal pigment epithelium (RPE) responsible for the visual cycle[2,3,6,7]. RPE65 plays a pivotal role in the conversion of all-*trans*-retinyl esters to 11-*cis*-retinal, a key step in the regeneration of rhodopsin and the maintenance of photoreceptor function[8–11]. In *Rpe65*$^{-/-}$ mice, the absence of functional RPE65 leads to disruption of the retinoid cycle, resulting in photoreceptor degeneration and severe visual impairment[12,13]. In humans, more than 100 mutations in *RPE65* have been identified as causative for LCA, highlighting the importance of this gene in retinal health[14–19]. However, the spectrum of *RPE65* mutations and their associated phenotypes in the Chinese population remains poorly characterized[20].

In this study, we identified two Chinese boys (aged 14 and 5 years) from the same family with compound heterozygous pathogenic variations in *RPE65* (p.Glu399*/p.Pro467Ala). Both brothers exhibited the classic symptoms of LCA, including night blindness and poor vision, as well as white spot lesions distributed throughout the retina—a phenotype previously reported in other RPE65-deficient models such as the rd12 mouse[21]. Although the p.Pro467Ala variation has been reported in humans[15,20], its direct disease-causing role *in vivo* remains unclear. Notably, the p.Glu399* variation and its associated phenotype have not been previously reported in the literature, suggesting a unique genetic and clinical profile in this family.

To investigate the functional consequences of the p.Pro467Ala mutation, we generated a knock-in mouse model harboring this variant. We hypothesized that this mutation might disrupt not only the visual cycle but also the neurotrophic signaling pathways critical for inner retinal integrity. Further transcriptomic and immunohistochemical analyses were performed to examine the expression of Vgf, a neurotrophic factor known to be expressed in the inner retina. Additionally, we sought to determine whether intravitreal administration of AQEE-30 very 4 d, a VGF nerve growth factor inducible (VGF)-derived neuroprotective peptide, could offer therapeutic benefit in RPE65-associated retinopathy. Our findings aim to expand the pathological spectrum of RPE65-related disease beyond the photoreceptors to include inner retinal neurons and provide a rationale for exploring neuroprotective strategies targeting VGF signaling to preserve retinal integrity in LCA.

This study aimed to characterize the pathological spectrum of RPE65-related disease beyond the photoreceptors to include the inner retinal neurons and evaluate neuroprotective strategies targeting VGF signaling to preserve retinal integrity in LCA.

Materials and methods

Human subjects and clinical evaluation

This study included two male Chinese siblings (aged 5 and 14 years at initial presentation) from a single family who presented

https://doi.org/10.48130/vns-0026-0035

with night blindness and visual impairment. The study protocol was reviewed and approved by the Clinical Research Ethics Committee of Changsha Maternal and Child Health Hospital (No. EC-20240625-17) and adhered to the tenets of the Declaration of Helsinki. Written informed consent was obtained from the parents as legal guardians and sample donors, and assent from the 14-year-old subject. The family was counseled on potential incidental findings from whole-exome sequencing prior to enrollment. All data were de-identified and stored securely. Clinical evaluations included comprehensive ophthalmic examinations, fundus photography, and electroretinography (ERG) performed according to the International Society for Clinical Electrophysiology of Vision (ISCEV) standards. Peripheral blood samples were collected for genomic DNA extraction. Whole-exome sequencing (WES) was performed to identify candidate variants, which were subsequently validated by Sanger sequencing in the probands in samples from the subjects and their parents to confirm inheritance patterns and segregation.

Breeding and genotyping of mice

The *Rpe65* p.Pro467Ala mutation was introduced into C57BL/6J background mice by Shanghai Southern Model Biotechnology Co., Ltd. The offspring were genotyped to identify carriers, and homozygous mice were generated through crossbreeding. Mice were housed under a 12-h light/12-h dark cycle (800 lux room light). The animal experiment was approved by the Biomedical Research Ethics Committee of Hunan Normal University (No. 2024-096).

Generation of *Rpe65* p.Pro467Ala knock-in mice

The *Rpe65* p.Pro467Ala (c.1399C>G) knock-in mouse model was generated in a pure C57BL/6J background by Shanghai Southern Model Biotechnology Co., Ltd. (Shanghai, China) using clustered regularly interspaced short palindromic repeats (CRISPR)/CRISPR-associated protein 9 (Cas9)-mediated homology-directed repair (HDR). A single-guide RNA (sgRNA) targeting exon 13 of mouse *Rpe65* (5'-GGAAGCTCTTGGTGGTGGTG-3'; protospacer adjacent motif [PAM]: 5'-TGG-3') was designed to position the Cas9 cleavage site 8 bp upstream of nucleotide c.1399. A 2.8-kb double-stranded DNA donor plasmid was constructed containing (1) a 1.2-kb 5' homology arm, (2) the c.1399 C>G point mutation (resulting in p.Pro467Ala substitution), (3) a loxP-flanked neomycin resistance (Neo^r) cassette inserted into intron 13 for positive selection, and (4) a 1.2-kb 3' homology arm.

Cas9 mRNA (100 ng/μL), sgRNA (50 ng/μL), and the donor plasmid (5 ng/μL) were co-injected into the pronuclei of fertilized C57BL/6J zygotes. The F0 founders were screened by polymerase chain reaction (PCR) using primers flanking the insertion site (forward: 5'-GCTGGA TGAGAAGGAGAAGG-3'; reverse: 5'-CCTCCA-GAAGGAGCTTCTGG-3'), yielding a 465-bp product for the mutant allele versus 402 bp for the wild-type allele. Sanger sequencing confirmed the precise incorporation of c.1399 C>G without indels at the target site or predicted off-target loci.

Positive founders were crossed with C57BL/6J-Tg (cyclization recombination enzyme [Cre]) 1Jxm/J mice (The Jackson Laboratory, #003376) to excise the Neo^r cassette via Cre-mediated recombination. Offspring retaining the point mutation but lacking Neo^r were identified by PCR (loss of the neo-specific band at 650 bp) and sequencing validation. The line was backcrossed to C57BL/6J for > 8 generations to eliminate potential off-target effects. Homozygous mutants were viable, fertile, and maintained as an inbred colony. All experimental mice were genotyped using allele-specific PCR with the primers described above. The mutant strain has been deposited in the China Mouse Genome Informatics database (CMGI ID: CMG-2022-RPE65-P467A).

Histology

Eyeballs from mutant and control mice were collected after anesthesia and fixed overnight in 4% paraformaldehyde (PFA) at 4 °C, followed by paraffin embedding.

For toluidine blue staining, anesthetized mice were perfused with 4% paraformaldehyde in phosphate-buffered saline (PBS). The eyes were embedded in JB-4 plastic, and 5-μm sections were prepared. The sections were dewaxed and rehydrated as follows:

(1) Immersion in Xylene I, II, and III for 5 min each;

(2) Soaking in anhydrous ethanol, 95% ethanol, and 75% ethanol for 1 min each;

(3) Rinsing with tap water for a few seconds.

Toluidine blue solution was applied for 20–30 min, followed by rinsing under running water to remove excess dye. Color separation was performed using 95% ethanol, with the separation effect monitored under a microscope. Sections were dehydrated in anhydrous ethanol for 1 min, cleared in xylene three times (1–2 min each), and mounted with neutral gum.

Morphometric analysis of retinal layer thickness

To quantitatively assess the retinal layer's thickness, whole eyes were serially sectioned along the optic nerve axis at approximately 200-μm intervals to cover the entire retina. From each section, three representative fields of view were imaged: The central region (corresponding to the thickest part of the retina, typically near the optic disc) and two peripheral regions located approximately ± 1 mm from the center. The thickness (in micrometers) of individual retinal layers—including the outer segments (OSs), the outer nuclear layer (ONL), the outer plexiform layer (OPL), the inner nuclear layer (INL), the inner plexiform layer (IPL), and the ganglion cell layer (GCL)—was measured using ImageJ software (National Institutes of Health [NIH], Bethesda, MD, USA) in a blinded manner. For each animal, at least three sections were analyzed, with three fields per section; the mean value across all measurements was used as the final thickness for that animal. Statistical comparisons between groups were performed using unpaired Student's *t*-test or one-way analysis of variance (ANOVA), as appropriate.

Drug administration

AQEE-30 (HY-P11192 MedChemExpress LLC, Shanghai, China), a VGF peptide, was dissolved in PBS to a concentration of 50 μM/2 μL. Under a surgical microscope, a 33-gauge needle was inserted through the sclera 0.5 mm posterior to the limbus, and 2 μL of the solution was slowly injected into the vitreous cavity. Control eyes received PBS injections. AQEE-30 (50 μM, 2 μL/eye) was administered via intravitreal injection once every 4 d for a total of 30 d[22].

Transcriptome sequencing and bioinformatic analysis

Total RNA was extracted from whole retinas of 8-week-old *Rpe65* p.Pro467Ala−/− and wild-type (WT) mice (n = 4 biological replicates per group) using TRIzol reagent (Invitrogen, Carlsbad, CA, USA) according to the manufacturer's protocol. RNA integrity was verified using an Agilent 2100 Bioanalyzer (RNA integrity number > 8.0). Libraries were prepared with the NEBNext Ultra™ RNA Library Prep Kit for Illumina (New England Biolabs [NEB], Ipswich, MA, USA)

and sequenced on an Illumina NovaSeq 6000 platform to generate 150-bp paired-end reads (average depth: 30 million reads/sample). Raw reads were processed using Trimmomatic (v0.39) to remove adapters and low-quality bases (Q < 20). Clean reads were aligned to the mouse reference genome (GRCm39) using HISAT2 (v2.2.1) with the default parameters. Gene expression was quantified by featureCounts (v2.0.1), and differential expression analysis was conducted using DESeq2 (v1.34.0) in R (v4.2.1). Genes with $|\log_2$ fold change (FC)$|$ > 1 and an adjusted p-value < 0.05 (Benjamini–Hochberg correction) were considered to be differentially expressed. Functional enrichment analysis was performed using clusterProfiler (v4.2.2) for Gene Ontology (GO) and Kyoto Encyclopedia of Genes and Genomes (KEGG) pathways.

Quantitative real-time polymerase chain reaction

cDNA was synthesized from 1μg total RNA using the PrimeScript™ RT Master Mix (Takara, Kyoto, Japan). Quantitative real-time polymerase chain reaction (qPCR) was performed on a QuantStudio™ 5 Real-Time PCR System (Thermo Fisher Scientific, Waltham, MA, USA) with TB Green™ Premix Ex Taq™ II (Takara). The reactions (20 μL) contained 10 μL SYBR Green mix, 0.8 μL of forward/reverse primers (10 μM), 2 μL complementary DNA (cDNA) template, and 6.4 μL nuclease-free water. The thermal cycling conditions were 95 °C for 30 s, then 40 cycles of 95 °C for 5 s and 60 °C for 30 s, followed by melt curve analysis. Primers were designed using Primer-BLAST with amplicon sizes of 80–150 bp. *Gapdh* served as the reference gene, validated for stable expression across genotypes (geNorm M < 0.5). Relative expression was calculated using the $2^{-\Delta\Delta C_T}$ method with polymerase chain reaction (PCR) efficiency correction (90%–110% efficiency confirmed by standard curves).

Statistical analysis

All quantitative data are presented as the mean ± standard error of the mean (SEM). The sample size was determined on the basis of a power analysis (α = 0.05, β = 0.2) using GPower 3.1, with n = 6 mice per experimental group (wild-type, p.Pro467Ala homozygous untreated, and p.Pro467Ala homozygous + AQEE-30) to ensure ≥ 80% power for detecting biologically relevant differences in retinal layer thickness. The normality of the data's distribution was assessed using the Shapiro–Wilk test (p > 0.05 for all variables), and the homogeneity of variance was confirmed by Levene's test. For comparisons between two groups (e.g., WT vs. mutant), unpaired two-tailed Student's t-test was applied. For comparisons across three or more groups (e.g., measurements of layer thickness), one-way analysis of variance (ANOVA) was performed, followed by Tukey's honest significant difference (HSD) *post hoc* test for pairwise comparisons with adjustment for multiple testing. Statistical significance was defined as p < 0.05, with exact p-values reported in the figures where possible; asterisks denote p < 0.05 (*), p < 0.01 (**), and p < 0.001 (***). All statistical analyses were performed using GraphPad Prism 9.0 (GraphPad Software, San Diego, CA, USA) and R version 4.2.1 (R Foundation for Statistical Computing, Vienna, Austria). Blinded morphometric measurements were independently verified by two investigators, with inter-rater reliability assessed by the intraclass correlation coefficient (ICC > 0.95).

Immunofluorescence staining

Paraffin-embedded retinal sections (5 μm) were deparaffinized, rehydrated, and subjected to antigen retrieval in 10 mM sodium citrate buffer (pH 6.0) at 95 °C for 20 min. Sections were blocked with 5% normal goat serum (NGS) in PBS containing 0.3% Triton X-100 for 1 h at room temperature. Primary antibodies were applied overnight at 4 °C: Rabbit anti-VGF antibody (1:200, Abcam ab229748, Abcam, Cambridge, UK) and mouse anti-glial fibrillary acidic protein (GFAP) antibody (1:500; Cat# MAB360, Millipore, Burlington, MA, USA). After washing, sections were incubated with Alexa Fluor 488-conjugated goat anti-rabbit immunoglobulin (IgG) (1:500; Cat# A-11034) and Alexa Fluor 594-conjugated goat anti-mouse IgG (1:500; Cat# A-11005; both from Thermo Fisher Scientific) for 1 h at room temperature in the dark. Nuclei were counterstained with 4′,6-diamidino-2-phenylindole (DAPI) (1 μg/mL; Cat# D1306, Thermo Fisher Scientific). Sections were mounted with ProLong™ Diamond Antifade Mountant (Cat# P36961, Thermo Fisher Scientific). Images were acquired using a Zeiss LSM 900 confocal microscope (63× oil objective, numerical aperture [NA] = 1.4) with identical laser power and gain settings across samples.

Results

The *RPE65* p.Glu399*/p.Pro467Ala compound heterozygous variant is associated with night blindness and retinal degeneration

Both brothers (aged 14 and 5 years) exhibited night blindness. WES revealed that each parent carried a single *RPE65* mutation: One parent harbored p.Glu399*, and the other carried p.Pro467Ala. Both brothers inherited both variants, resulting in a compound heterozygous genotype (Fig. 1a). Unlike classic vitelliform maculopathy, these patients presented with diffuse white spot lesions, a pattern reminiscent of that observed in the *Rpe65*^{rd12} mouse model[21], though distinct in its distribution and clinical context. (Fig. 1b–e), and widespread photoreceptor and inner retinal dysfunction in the patients (Supplementary Fig. S1).

Rpe65 p.Pro467Ala mutant mice exhibit a disordered GCL

Although *Rpe65* p.Glu399* is a novel nonsense mutation, the pathogenicity of p.Pro467Ala in causing LCA remains unclear. To investigate this, we generated *Rpe65* p.Pro467Ala mutant mice (Fig. 2d). At 12 weeks, toluidine blue-stained retinal sections revealed significant reductions in the photoreceptors' OSs, ONL, OPL, and INL (Fig. 2a–c). Interestingly, in homozygous *Rpe65* p.Pro467Ala mice, the GCL exhibited disorganization, with irregularly shaped nuclei and solid, elongated abnormal nuclei in the affected regions (Fig. 2a, b).

Decreased VGF signaling in the GCL of Rpe65 p.Pro467Ala mice

To identify the signaling pathways underlying the GCL phenotype, we performed transcriptome analysis and qPCR experiments using eyes from 8-week-old mice. Consistent with our histological observations, RNA sequencing revealed significantly decreased expression of several genes associated with retinal function, including *Vgf*, *Cndp3*, *Gngt2*, *Pde6h*, *Pde6c*, *Cnga3*, *Guca1a*, and *Gnat2*, in the eyes of p.Pro467Ala mutant mice (Fig. 3a).

qPCR validation confirmed the downregulation of these genes, consistent with the transcriptomic data (Fig. 3b). Immunofluorescence staining revealed markedly reduced VGF protein levels in mutant retinas, with the signal predominantly localized to the INL, corresponding to Müller glial cell bodies, and weaker expression in astrocytic processes surrounding the GCL (Fig. 3c, d). Transcriptomic and immunofluorescence analyses revealed the significant downregulation of Vgf/VGF in mutant retinas (Fig. 3a–d). Concurrently, structural disorganization of the GCL was observed in the

https://doi.org/10.48130/vns-0026-0035

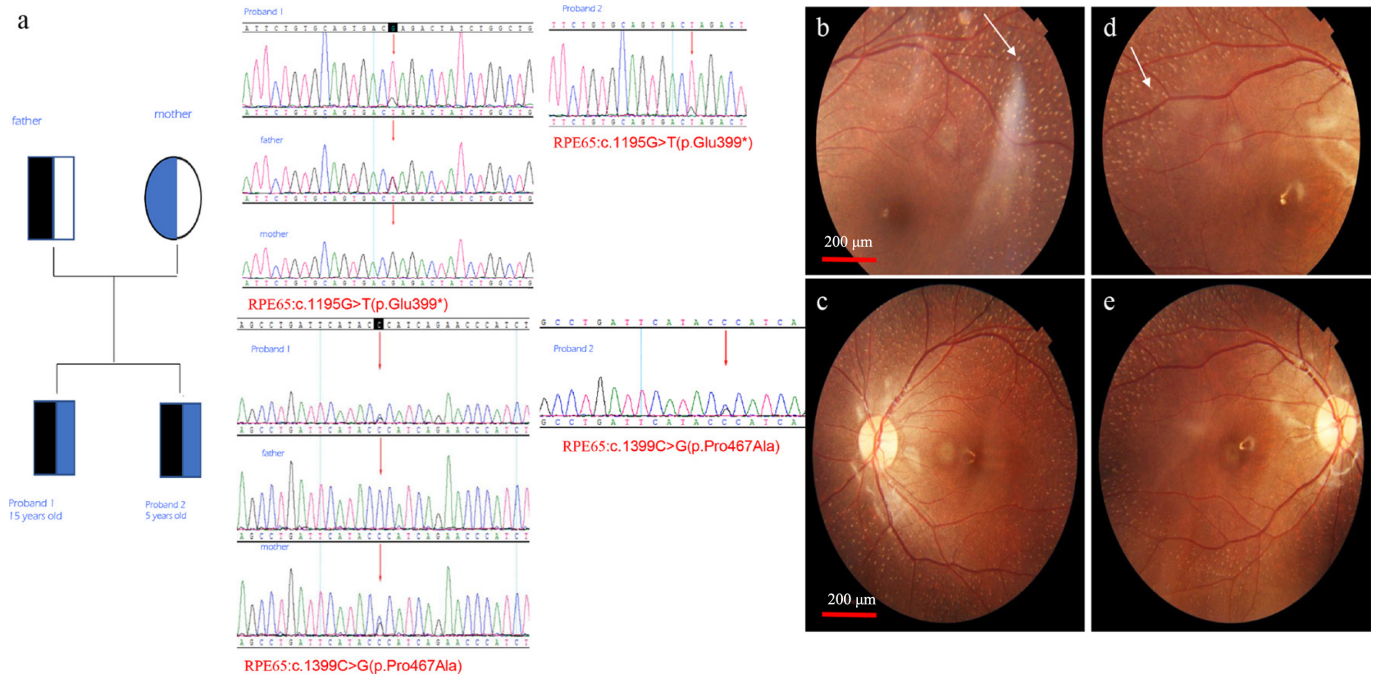

Fig. 1 Compound heterozygous *RPE65* mutations (p.Glu399*/p.Pro467Ala) associated with atypical white spot lesions in two Chinese siblings with LCA. (a) Pedigree analysis and Sanger sequencing confirmed compound heterozygosity: p.Glu399* (c.1195G>T) inherited paternally and p.Pro467Ala (c.1399C>G) maternally. (b)–(e) Fundus photographs showing numerous white dot-like lesions distributed throughout the posterior pole, distinct from classic vitelliform maculopathy.

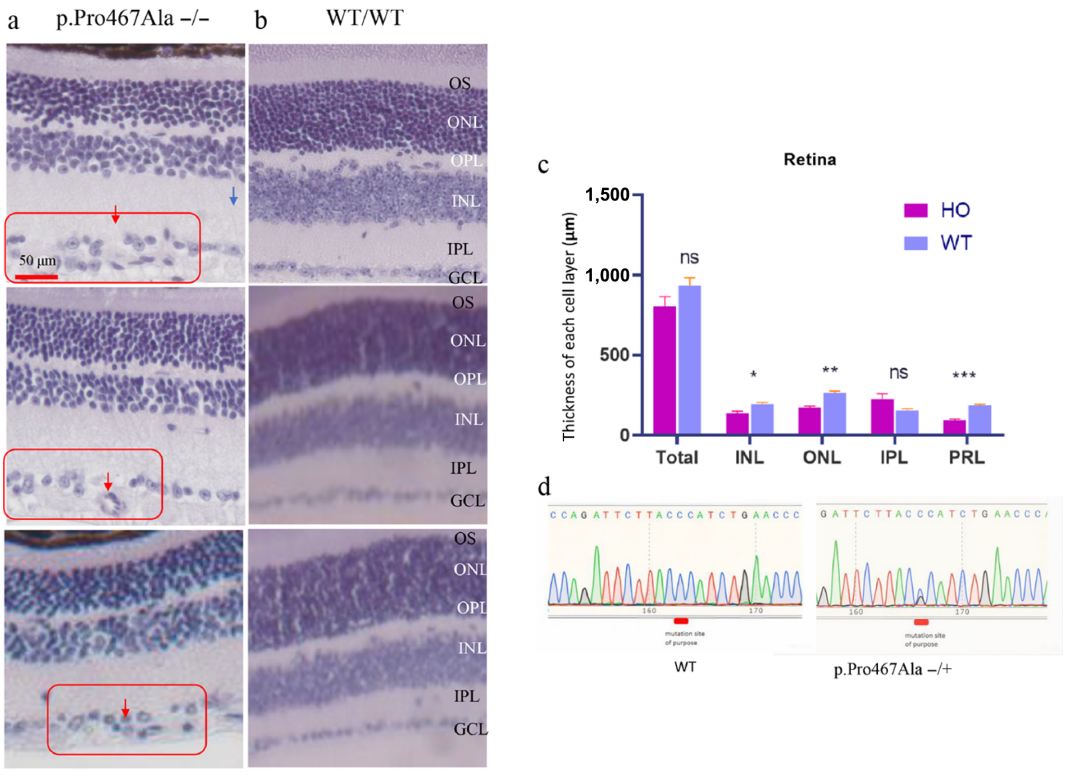

Fig. 2 Toluidine blue-stained retinal cross-sections show retinal degeneration and disorganization of the GCL in *Rpe 65* p.Pro467Ala homozygous mice at 12 weeks of age. (a) Representative image of the mutant retina showing distinct areas of cellular disorganization within the GCL, as indicated by the red boxes and red arrows. In contrast, other regions of the GCL exhibit a relatively normal cellular arrangement (blue arrow). Scale bar: 50 μm. (b) Representative image of the WT retina, demonstrating a well-organized and uniformly aligned GCL ($n = 6$). (c) Quantitative analysis of the thickness of individual retinal layers in both the mutant and control (WT) groups. Data are presented as the mean ± SEM. Statistical significance was determined by unpaired Student's *t*-tests (* $p < 0.05$, ** $p < 0.01$, *** $p < 0.001$). Scale bars: 50 μm. OS, outer segment; ONL, outer nuclear layer; INL, inner nuclear layer; IPL, inner plexiform layer; OPL, outer plexiform layer; GCL, ganglion cell layer; PRL, photoreceptor layer, which includes both OSs and inner segments (IS); HO, homozygous; OPL, outer plexiform layer. (d) Sanger sequencing confirmed the presence of the c.1399C>G nucleotide substitution at the DNA level.

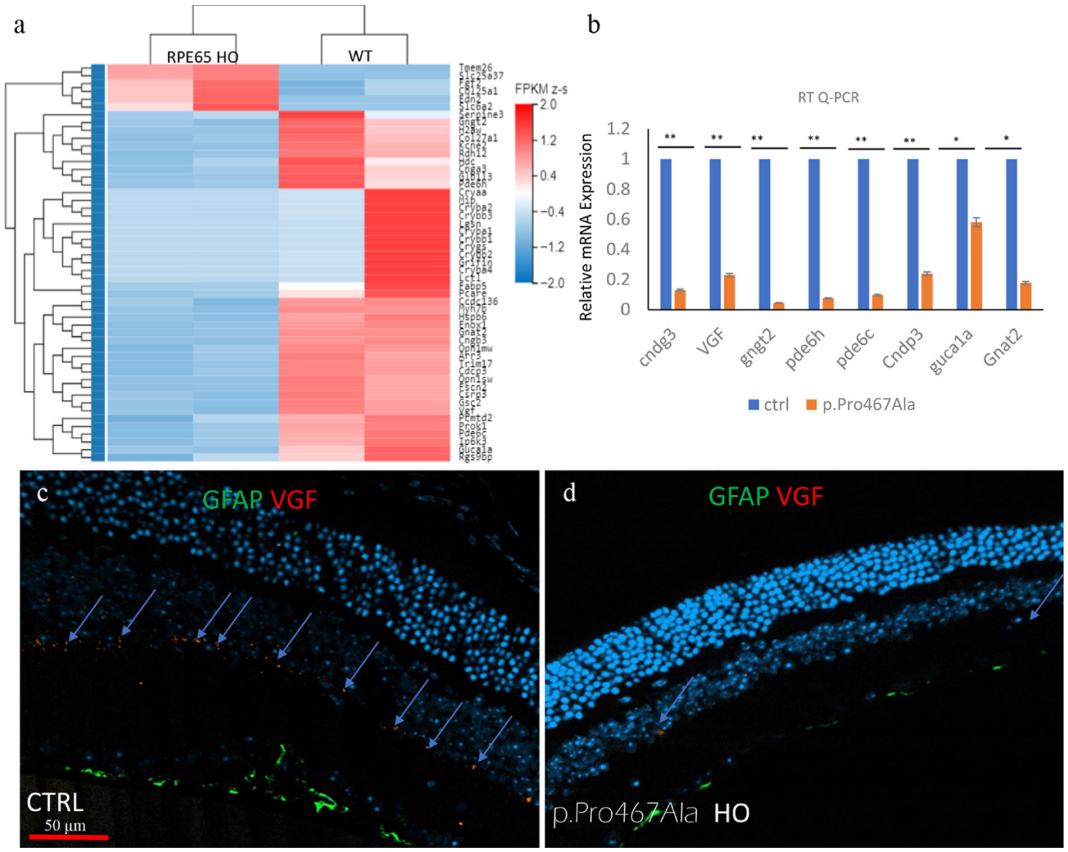

Fig. 3 Transcriptomic analysis reveals downregulation of retinal functional genes and reduced VGF expression in the GCL of *Rpe65* p.Pro467Ala homozygous mice. (a) Heatmap of RNA sequencing data showing decreased expression of phototransduction- and neuronal function- related genes, including *Vgf*, *Cndp3*, *Gngt2*, *Pde6h*, *Pde6c*, *Cnga3*, *Guca1a*, and *Gnat2*, in mutant retinas. (b) qPCR validation confirmed significant downregulation of these genes, consistent with transcriptome profiling. (c,d) Immunofluorescence staining demonstrates markedly reduced VGF signal (red) predominantly in the INL and in GFAP-positive astrocytic processes surrounding the GCL of (c) wild-type controls compared with (d) mutant mice (nuclei counterstained with DAPI in blue), supporting a glia-derived, non-cell-autonomous role of VGF in GCL pathology.

same cohort of mutant mice (Fig. 2). This reduction in glia-derived VGF with structural abnormalities of the GCL suggested a non-cell-autonomous role of VGF signaling in maintaining inner retinal integrity.

AQEE-30, a VGF peptide, alleviates the GCL phenotype in *Rpe65* p.Pro467Ala mice

To determine whether GCL disorganization in *Rpe65* p.Pro467Ala mutant mice is mediated by impaired VGF signaling, we performed a rescue experiment using AQEE-30, a neuroprotective peptide derived from the VGF precursor[22]. AQEE-30 (50 μM, 2 μL/eye) was administered via intravitreal injection to 8-week-old *Rpe65* p.Pro467Ala homozygous mice once every 4 d for a total of 30 d. Hematoxylin and eosin (H&E) staining revealed that AQEE-30 treatment significantly ameliorated the structural disruption of the GCL in mutant mice (Fig. 4a, b). suggesting that enhancing VGF-related signaling may confer trophic support to the inner retina, even if VGF is not directly expressed in retinal ganglion cells (RGCs).

Discussion

RPE65 is well known for its critical role in retinoid metabolism, maintenance of the photoreceptor layer, rod photoreceptors' function, rodsopsin phosphorylation, and cone photoreceptors' survival[8,9,23]. In mammals, a small subset of retinal ganglion cells (RGCs), known as intrinsically photosensitive retinal ganglion cells (ipRGCs), are responsible for non-image-forming visual functions. These ipRGCs primarily project to the suprachiasmatic nucleus

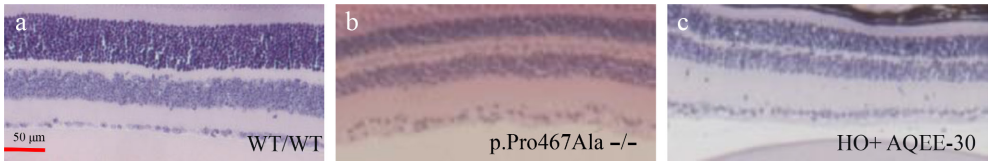

Fig. 4 AQEE-30 treatment ameliorates disorganization of the GCL in *p.Pro467Ala* homozygous mice. Hematoxylin and eosin (H&E) staining of retinal sections from 8-week-old mice after intravitreal administration of AQEE-30 (50 μM, 2 μL/eye, once every 4 d for 30 d). (a) AQEE-30-treated mutant mice showed improved structural integrity of the GCL. (b) Untreated *Rpe65* Pro467Ala homozygous control mice exhibit marked GCL disarray. Scale bar: 50 μm. These findings suggest that the VGF-derived peptide AQEE-30 exerts protective effects on retinal ganglion cells in the context of the *RPE65* mutation.

https://doi.org/10.48130/vns-0026-0035

(SCN), the intergeniculate leaflet, and the olivary pretectal nucleus (OPN) of the brain[23–25]. Previous studies have demonstrated that ipRGCs are largely unaffected by ablation of RPE65. This is because the melanopsin-dependent photocycle functions independently of the canonical visual retinoid cycle, allowing ipRGCs to maintain intact photic sensitivity even in the absence of functional RPE65[26].

In our study, we observed that *Rpe65* p.Pro467Ala homozygous mice exhibited intermittent disorganization in the GCL, characterized by an irregular nuclear morphology and focal loss of cellular alignment. Although the identity of the affected neurons remains to be fully determined, these disordered regions may involve subsets of RGCs, potentially including ipRGCs. The white dot-like lesions observed in the probands' fundus could reflect focal inner retinal atrophy or gliosis secondary to such neuronal dysfunction. The presence of retinal white spots in our patients aligns with prior observations in *Rpe65*-null mice[21], where such lesions correlated with the accumulation of liquid droplets in the RPE and photoreceptor degeneration, rather than primary ganglion cell pathology.

Consistent with Takeuchi et al.[22], our immunostaining experiment confirmed that VGF is expressed predominantly in thee Müller glia (INL) and astrocytes, not in the RGC somata themselves. The observed GCL pathology likely reflects the loss of trophic support from glia-derived VGF peptides (e.g., AQEE-30) that normally diffuse to the neighboring neurons. This non-cell-autonomous mechanism explains why intravitreal AQEE-30 administration—despite minimal direct VGF expression in the RGCs—significantly ameliorated disorganization of the GCL.

Although Métrailler et al.[27] reported extracellular signal-regulated kinase 1/2 (ERK1/2) activation and GFAP upregulation in the GCL of Rpe65$^{-/-}$ mice, suggesting secondary stress responses in the inner retinal neurons, our knock-in model revealed primary structural disorganization of the GCL's nuclear architecture. This distinction may reflect mutation-specific effects of the p.Pro467Ala variant versus complete RPE65 ablation, and highlights VGF signaling deficiency as a previously unrecognized contributor to inner retinal pathology in RPE65-associated disease.

Though our homozygous p.Pro467Ala knock-in model successfully isolated the pathogenic contribution of this missense variant and revealed its specific impact on inner retinal architecture, we acknowledge an important limitation: The patients harbor a compound heterozygous genotype (p.Glu399*/p.Pro467Ala) rather than homozygosity for p.Pro467Ala. The p.Glu399* nonsense allele is predicted to trigger nonsense-mediated decay and a complete loss of RPE65 protein, whereas p.Pro467Ala likely permits protein expression with impaired isomer hydrolase activity. This allelic combination may produce a more severe visual cycle defect than the homozygous missense state modeled here. Nevertheless, our approach was deliberately chosen to dissect the pathological mechanisms of the variant of uncertain significance (p.Pro467Ala) without confounding effects from a null allele, a strategy with a precedent in monogenic retinal disease research[28]. Future generation of compound heterozygous mice will be valuable to fully recapitulate the human genotype and determine whether the inner retinal pathology is exacerbated in the presence of a complete loss-of-function allele.

Given the incomplete understanding of inner retinal pathology in RPE65-associated disease, we sought to characterize the functional consequences of the p.Pro467Ala mutation using a knock-in mouse model. We hypothesized that this clinically relevant missense variant might induce pathology beyond canonical photoreceptor degeneration, potentially involving neurotrophic signaling pathways in the inner retinal neurons.

Though over 100 pathogenic variants of RPE65 have been documented worldwide[29], the mutation spectrum and associated phenotypic variability in Chinese LCA patients remain incompletely characterized[20,30]. Notably, emerging evidence suggests that RPE65 dysfunction may extend beyond photoreceptor degeneration to affect the inner retinal neurons[27], though the underlying mechanisms remain elusive. In this study, we identified a Chinese family harboring a novel compound heterozygous RPE65 genotype (p.Glu399*/p.Pro467Ala) associated with atypical retinal manifestations. To investigate the pathogenic mechanisms of the p.Pro467Ala variant, we generated a knock-in mouse model and hypothesized that this mutation might disrupt not only the visual cycle but also the neurotrophic signaling pathways critical for inner retinal integrity. Our integrated approach combining clinical phenotyping, histopathological analysis, transcriptomics, and targeted peptide intervention aimed to delineate novel pathological mechanisms and identify potential therapeutic targets for RPE65-associated retinopathy.

A critical observation in our therapeutic intervention is the layer-specific neuroprotection conferred by AQEE-30: Although the GCL's structural integrity was significantly ameliorated, the photoreceptors' OSs and ONL remained severely degenerated despite treatment. This selective rescue aligns precisely with the spatial expression pattern of VGF itself, predominantly in the Müller glia (INL) and astrocytic processes surrounding the GCL, but absent from photoreceptors[22]. Mechanistically, AQEE-30 (a *C*-terminal VGF-derived peptide) likely acts through non-cell-autonomous trophic support. Secreted from inner retinal glia, it diffuses locally to the neighboring ganglion cells and amacrine neurons, activating pro-survival pathways (e.g., phosphoinositide 3-kinase [PI3K]/protein kinase B [AKT]) that preserve the nuclear architecture and cellular alignment. In contrast, photoreceptor degeneration in Rpe65 deficiency stems from a cell-autonomous biochemical defect: The inability to regenerate 11-*cis*-retinal because of impaired isomer hydrolase activity in the RPE. Since AQEE-30 does not restore visual chromophore recycling or correct the primary enzymatic deficit, it cannot prevent the inexorable loss of photoreceptors. This dichotomy underscores a fundamental principle: Neuroprotective peptides targeting inner retinal signaling pathways may serve as adjunctive therapy to preserve ganglion cells' function in RPE65-associated LCA but must be combined with approaches that address the root cause (e.g., gene therapy with voretigene neparvovec) for comprehensive retinal rescue.The ability of exogenous AQEE-30 to ameliorate disorganization of the GCL suggests that impaired VGF signaling may contribute to inner retinal pathology in this model, though the precise cellular mechanisms remain to be elucidated.

Ethical statements

The animal experiment was approved by the Biomedical Research Ethics Committee of Hunan Normal University (Approval No. 2024-096; dated March 11, 2024). The research followed the 'Replacement, Reduction, and Refinement' principles to minimize harm to animals. The clinical study was approved by the Clinical Research Ethics Committee of Changsha Maternal and Child Health Hospital (Approval No. EC-20240625-17; dated June 25, 2024). Written informed consent was obtained from the parents (as guardians and sample donors) and assent from the 14-year-old subject, with pre-test counseling on incidental WES findings. All data were de-identified and stored securely.

Author contributions

The authors confirm their contributions to the paper as follows: conceptualized and drafted the initial manuscript, and reviewed and revised the manuscript: Wang S, Peng X; collected data, and reviewed and revised the manuscript: Yang J, Peng X, Hu X. All authors reviewed the results and approved the final version of the manuscript.

Data availability

Data generated or analyzed during this study are available from the corresponding author upon reasonable request.

Acknowledgments

This project is supported by the Project of Changsha Science and Technology Bureau (KH2201045), the Natural Science Foundation of Hunan Province (2023JJ30063), the Changsha Science and Technology Bureau natural science surface project (kq2202030), and the National Natural Science Foundation of China (32070817).

Conflict of interest

The authors declare that they have no conflict of interest.

Supplementary information This accompanies this paper online at: https://doi.org/10.48130/vns-0026-0035.

Dates

Received 10 November 2025; Revised 10 April 2026; Accepted 22 May 2026; Published online 10 August 2026

References

[1] Allikmets R. 2004. Leber congenital amaurosis: a genetic paradigm. *Ophthalmic Genetics* 25:67–79

[2] Apte RS. 2018. Gene therapy for retinal degeneration. *Cell* 173:5

[3] Bok D. 1993. The retinal pigment epithelium: a versatile partner in vision. *Journal of Cell Science* 1993:189–195

[4] Chacon-Camacho OF, Zenteno JC. 2015. Review and update on the molecular basis of Leber congenital amaurosis. *World Journal of Clinical Cases* 3:112–124

[5] Sahel JA. 2011. Spotlight on childhood blindness. *Journal of Clinical Investigation* 121:2145–2149

[6] Verma A, Perumalsamy V, Shetty S, Kulm M, Sundaresan P. 2013. Mutational screening of LCA genes emphasizing *RPE65* in south Indian cohort of patients. *PLoS One* 8:e73172

[7] Harris EW. 2001. Leber's congenital amaurosis and RPE65. *International Ophthalmology Clinics* 41:73–82

[8] Rohrer B, Goletz P, Znoiko S, Ablonczy Z, Ma JX, et al. 2003. Correlation of regenerable opsin with rod ERG signal in *Rpe65*$^{-/-}$ mice during development and aging. *Investigative Opthalmology & Visual Science* 44:310–315

[9] Feathers KL, Lyubarsky AL, Khan NW, Teofilo K, Swaroop A, et al. 2008. *Nrl*-knockout mice deficient in Rpe65 fail to synthesize 11-*cis* retinal and cone outer segments. *Investigative Opthalmology & Visual Science* 49:1126–1135

[10] Lyubarsky AL, Savchenko AB, Morocco SB, Daniele LL, Redmond TM, et al. 2005. Mole quantity of RPE65 and its productivity in the generation of 11-*cis*-retinal from retinyl esters in the living mouse eye. *Biochemistry* 44:9880–9888

[11] Redmond TM, Yu S, Lee E, Bok D, Hamasaki D, et al. 1998. Rpe65 is necessary for production of 11-*cis*-vitamin A in the retinal visual cycle. *Nature Genetics* 20:344–351

[12] Grimm C, Wenzel A, Hafezi F, Yu S, Redmond TM, et al. 2000. Protection of *Rpe65*-deficient mice identifies rhodopsin as a mediator of light-induced retinal degeneration. *Nature Genetics* 25:63–66

[13] Chen Y, Moiseyev G, Takahashi Y, Ma JX. 2006. *RPE65* gene delivery restores isomerohydrolase activity and prevents early cone loss in Rpe65$^{-/-}$ mice. *Investigative Ophthalmology & Visual Science* 47:1177–1184

[14] Abduljaleel Z. 2019. Comprehensive structure-function analysis of causative variants in retinal pigment epithelium specific 65 kDa protein associated Leber Congenital Amaurosis. *Non-coding RNA Research* 4:121–127

[15] Sinim Kahraman N, Öner A, Özkul Y, Dündar M. 2022. Frequency of *RPE65* gene mutation in patients with hereditary retinal dystrophy. *Turkish Journal of Ophthalmology* 52:270–275

[16] Feathers KL, Jia L, Khan NW, Smith AJ, Ma JX, et al. 2023. Gene supplementation in mice heterozygous for the D477G RPE65 variant implicated in autosomal dominant retinitis pigmentosa. *Human Gene Therapy* 34:639–648

[17] Vázquez-Domínguez I, Duijkers L, Fadaie Z, Alaerds ECW, Post MA, et al. 2022. The predicted splicing variant c. 11+5G>A in *RPE65* leads to a reduction in mRNA expression in a cell-specific manner. *Cells* 11:3640

[18] Bjeloš M, Bušić M, Ćurić A, Šari ć B, Bosnar D, et al . 2022. *RPE65* c.353G>A, p.(Arg118Lys): a novel point mutation associated with retinitis pigmentosa and macular atrophy. *International Journal of Molecular Sciences* 23:10513

[19] Pappalardo J, Heath Jeffery RC, Thompson JA, Chelva E, Pham Q, et al. 2021. A novel phenotype in a family with autosomal dominant retinal dystrophy due to c. 1430A > G in retinoid isomerohydrolase (*RPE65*) and c. 37C > T in bestrophin 1 (*BEST1*). *Documenta Ophthalmologica* 143:61–73

[20] Zhong Z, Rong F, Dai Y, Yibulayin A, Zeng L, et al. 2019. Seven novel variants expand the spectrum of *RPE65*-related Leber congenital amaurosis in the Chinese population. *Molecular Vision* 25:204–214

[21] Pang JJ, Chang B, Hawes NL, Hurd RE, Davisson MT, et al. 2005. Retinal degeneration 12 (rd12): a new, spontaneously arising mouse model for human Leber congenital amaurosis (LCA). *Molecular Vision* 11:152–162

[22] Takeuchi H, Inagaki S, Morozumi W, Nakano Y, Inoue Y, et al. 2018. VGF nerve growth factor inducible is involved in retinal ganglion cells death induced by optic nerve crush. *Scientific Reports* 8:16443

[23] Fan J, Rohrer B, Frederick JM, Baehr W, Crouch RK. 2008. *Rpe65*$^{-/-}$and *Lrat*$^{-/-}$Mice: comparable models of leber congenital amaurosis. *Investigative Opthalmology & Visual Science* 49:2384–2389

[24] Berson DM, Dunn FA, Takao M. 2002. Phototransduction by retinal ganglion cells that set the circadian clock. *Science* 295:1070–1073

[25] Hattar S, Liao HW, Takao M, Berson DM, Yau KW. 2002. Melanopsin-containing retinal ganglion cells: architecture, projections, and intrinsic photosensitivity. *Science* 295:1065–1070

[26] Tu DC, Owens LA, Anderson L, Golczak M, Doyle SE, et al. 2006. Inner retinal photoreception independent of the visual retinoid cycle. *Proceedings of the National Academy of Sciences of the United States of America* 103:10426–10431

[27] Métrailler S, Emery M, Schorderet DF, Cottet S, Roduit R. 2013. ERK1/2 pathway is activated in degenerated *Rpe65*-deficient mice. *Experimental Eye Research* 116:86–95

[28] Cideciyan AV, Jacobson SG, Beltran WA, Sumaroka A, Swider M, et al. 2013. Human retinal gene therapy for Leber congenital amaurosis shows advancing retinal degeneration despite enduring visual improvement. *Proceedings of the National Academy of Sciences of the United States of America* 110:E517–E525

[29] Motta FL, Martin RP, Porto FBO, Wohler ES, Resende RG, et al. 2020. Pathogenicity reclassification of *RPE65* missense variants related to leber congenital amaurosis and early-onset retinal dystrophy. *Genes* 11:24

[30] Li S, Xiao X, Yi Z, Sun W, Wang P, et al. 2020. RPE65 mutation frequency and phenotypic variation according to exome sequencing in a tertiary centre for genetic eye diseases in China. *Acta Ophthalmologica* 98:e181–e190